Physics Letters B 747 (2015) 331–338

Contents lists available at ScienceDirect

Physics Letters B

www.elsevier.com/locate/physletb

Direct detection constraints on dark photon dark matter

Haipeng An [a], Maxim Pospelov [b,c], Josef Pradler [d,*], Adam Ritz [b]

[a] Walter Burke Institute for Theoretical Physics, California Institute of Technology, Pasadena, CA 91125, United States
[b] Department of Physics and Astronomy, University of Victoria, Victoria, BC V8P 5C2, Canada
[c] Perimeter Institute for Theoretical Physics, Waterloo, ON N2J 2W9, Canada
[d] Institute of High Energy Physics, Austrian Academy of Sciences, Nikolsdorfergasse 18, 1050 Vienna, Austria

ARTICLE INFO

Article history:
Received 20 January 2015
Received in revised form 7 May 2015
Accepted 10 June 2015
Available online 11 June 2015
Editor: A. Ringwald

ABSTRACT

Dark matter detectors built primarily to probe elastic scattering of WIMPs on nuclei are also precise probes of light, weakly coupled, particles that may be absorbed by the detector material. In this paper, we derive constraints on the minimal model of dark matter comprised of long-lived vector states V (dark photons) in the 0.01–100 keV mass range. The absence of an ionization signal in direct detection experiments such as XENON10 and XENON100 places a very strong constraint on the dark photon mixing angle, down to $\mathcal{O}(10^{-15})$, assuming that dark photons comprise the dominant fraction of dark matter. This sensitivity to dark photon dark matter exceeds the indirect bounds derived from stellar energy loss considerations over a significant fraction of the available mass range. We also revisit indirect constraints from $V \to 3\gamma$ decay and show that limits from modifications to the cosmological ionization history are comparable to the updated limits from the diffuse γ-ray flux.

1. Introduction

The Standard Model of particle physics (SM) is known to be incomplete, in that it needs to be augmented to include the effects of neutrino mass. Furthermore, cosmology and astrophysics provide another strong motivation to extend the SM, through the need for dark matter (DM). Evidence ranging in distance and time scales from the horizon during decoupling of the cosmic microwave background (CMB) to sub-galactic distances points to the existence of 'missing mass' in the form of cold, non-baryonic DM. The particle (or, more generally, field theoretic) identity of dark matter remains a mystery—one that has occupied the physics community for many years.

While the 'theory-space' for DM remains enormous, several model classes can be broadly identified. Should new physics exist at or near the electroweak scale, a weakly interacting massive particle (WIMP) becomes a viable option. The WIMP paradigm assumes the existence of a relatively heavy particle (typically with a mass in the GeV to TeV range) having sizeable couplings to the SM. The self-annihilation into the SM regulates the WIMP cosmic abundance according to thermal freeze-out, and the observed relic density requires a weak-scale annihilation rate. The simplest models of this type also predict a significant scattering rate for WIMPs in the galactic halo on nuclei, when up to 100 keV of WIMP kinetic energy can be transferred to atoms, offering a variety of pathways for detection. Direct detection, as it has became known, is a rapidly growing field, with significant gains in sensitivity achieved in the last two decades, and with a clear path forward [1].

Alternatively, DM could be in the form of super-weakly interacting particles, with a negligible abundance in the early Universe, and generated through a sub-Hubble thermal leakage rate (also known as the 'freeze-in' process). Dark matter of this type is harder to detect directly, as the couplings to the SM are usually smaller than those of WIMPs by many orders of magnitude. Metastability of such states offers a pathway for the indirect detection of photons in the decay products, as is the case for metastable neutrino-like particles in the $O(10\ \text{keV})$ mass range (see, *e.g.* [2]). It was also pointed out in [3] that WIMP direct detection experiments are sensitive to bosonic DM particles with couplings of $O(10^{-10})$ or below, that could be called super-WIMPs (referring to the 'super-weak' strength of their SM interactions).

Finally, a completely different and independent class of models for dark matter involves light bosonic fields with an abundance generated via the vacuum misalignment mechanism [4–6]. In this class of models, DM particles emerge from a cold condensate-like state with very large particle occupation numbers, which can be well described by a classical field configuration. The mass and initial amplitude of the DM field defines its present energy density. The most prominent example in this class, the QCD axion, does

* Corresponding author.
E-mail address: josef.pradler@oeaw.ac.at (J. Pradler).

http://dx.doi.org/10.1016/j.physletb.2015.06.018

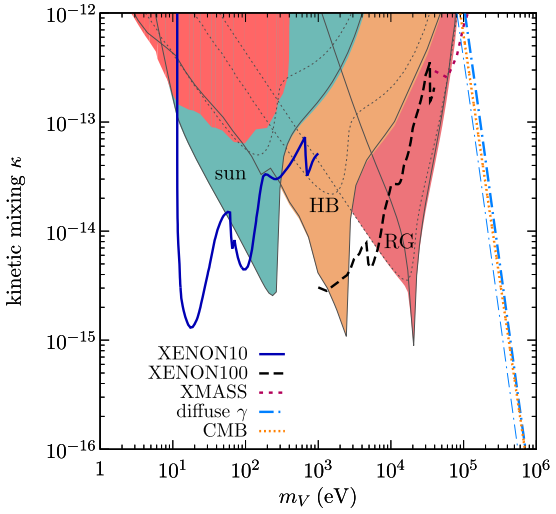

Fig. 1. A summary of constraints on the dark photon kinetic mixing parameter κ as a function of vector mass m_V (see Sections 2 and 3 for the details). The thick lines exclude the region above for dark photons with dark matter relic density. The solid (dashed) line is from XENON10 (XENON100); the limit from XMASS is taken from [25]. The dash-dotted lines show our newly derived constraints on the diffuse γ-ray flux from $V \to 3\gamma$ decays, assuming that decays contribute 100% (thick line) or 10% (thin line) to the observed flux. The thick dotted line is the corresponding constraint from CMB energy injection. Shaded regions depict (previously considered) astrophysical constraints that are independent of the dark photon relic density. The limits from anomalous energy loss in the sun (sun), horizontal branch stars (HB), and red giant stars (RG) are labeled. The shaded region that is mostly inside the solar constraint is the XENON10 limit derived from the solar flux [31].

have a non-vanishing interaction with SM fields, although other forms of 'super-cold' DM do not necessarily imply any significant coupling. While axion dark matter has been the focus of many experimental searches and proposals [7], other forms of super-cold dark matter have received comparatively less attention (see *e.g.* [8–10,13]). In the course of these latter investigations, and subsequent work, several experimental strategies for detecting such dark matter scenarios have been suggested [14–16].

Regarding the latter class of models, it is also possible to generate a dark matter abundance not only from a pre-existing condensate (vacuum misalignment) but gravitationally, during inflation, through perturbations in the field that carry finite wave number k [11]. Recent work [12] investigates this possibility for vector particles, reaching the conclusion that such mechanism avoids large-scale isocurvature constraints from CMB observations, and allows light vectors to be generated in sufficient abundance as viable dark matter candidates.

In this paper, we consider 'dark photon dark matter' generated through inflationary perturbations, or possibly other non-thermal mechanisms. While existing proposals to detect dark photons address the range of masses below $\mathcal{O}$(meV), we will investigate the sensitivity of existing WIMP-search experiments to dark photon dark matter with mass in the 10 eV–100 keV window. As we will show, the coupling constant of the dark photon to electrons, $e\kappa$, can be probed to exquisitely low values, down to mixing angles as low as $\kappa \sim O(10^{-15})$. Furthermore, sensitivity to this mixing could be improved with careful analysis of the 'ionization-only' signal available to a variety of DM experiments. The sensitivity of liquid xenon experiments to vector particles has already been explored in [17] and many experiments have already reported relevant analyses [18–25]. While we concentrate on the Stuckelberg-type mass for the vector field, our treatment of direct detection of V will equally apply to the Higgsed version of the model. Moreover, the existence of a Higgs field charged under $U(1)'$ opens up additional possibilities for achieving the required cosmological abundance of V.

The rest of this work is organized as follows. In Section 2 we introduce the dark photon model in some more detail, describe existing constraints, and reconsider indirect limits. In Section 3 we compile the relevant formulae for direct detection, confront the model with existing direct detection results and derive constraints on the mixing angle κ. The results are summarized in Fig. 1, which shows the new direct detection limits in comparison to various astrophysical constraints. In Section 4, we provide a general discussion of super-weakly coupled DM, and possible improvements in sensitivity to (sub-)keV-scale DM particles.

2. Dark photon dark matter

It has been well-known since 1980s that the SM allows for a natural UV-complete extension by a new massive or massless $U(1)'$ field, coupled to the SM hypercharge $U(1)$ via the kinetic mixing term [26]. Below the electroweak scale, the effective kinetic mixing of strength κ between the dark photon (V) and photon (A) with respective field strengths $V_{\mu\nu}$ and $F_{\mu\nu}$ is the most relevant,

$$\mathcal{L} = -\frac{1}{4}F_{\mu\nu}^2 - \frac{1}{4}V_{\mu\nu}^2 - \frac{\kappa}{2}F_{\mu\nu}V^{\mu\nu} + \frac{m_V^2}{2}V_\mu V^\mu + eJ_{\rm em}^\mu A_\mu, \quad (1)$$

where $J_{\rm em}^\mu$ is the electromagnetic current and m_V is the dark photon mass. This model has been under significant scrutiny over the last few years, as the minimal realization of one the few UV-complete extensions of the SM (portals) that allows for the existence of light weakly coupled particles [27]. For simplicity, we will consider the Stückelberg version of this vector portal, in which m_V can be added by hand, rather than being induced via the Higgs mechanism.

2.1. Cosmological abundance

Light vector particles with $m_V < 2m_e$ have multiple contributions to their cosmological abundance, such as (a) production through scattering or annihilation, $\gamma e^\pm \to Ve^\pm$ and $e^+e^- \to V\gamma$, possibly with sub-Hubble rates, (b) resonant photon-dark photon conversion, or (c) production from an initial dark photon condensate, as could be seeded by inflationary perturbations. Notice that if mechanisms (a) and (b) are the only sources that populate the DM, they are not going to be compatible with cold dark matter when $m_V \lesssim$ keV.

For mechanism (a), naive dimensional analysis suggests a dark photon interaction rate $\Gamma_{\rm int} \sim \kappa^2\alpha^2 n_e/s$, where n_e is the electron number density and $\sqrt{s}$ is the centre-of-mass energy. At temperatures $T \gg m_e$, where the number density of charge carriers is maximal, $n_e \sim T^3$, this production rate scales linearly with temperature, whereas the Hubble rate is a quadratic function of T. It follows that for sub-MeV mass dark vectors, the thermal production of V is maximized at $T \sim m_e$. However, simple parametric estimates of this kind may require refinement due to matter effects that alter the most naive picture. At finite temperature T, the in-medium effects can be cast into a modification of the mixing angle,

$$\kappa_{T,L}^2 = \kappa^2 \times \frac{m_V^4}{|m_V^2 - \Pi_{T,L}|^2}, \quad (2)$$

where $\Pi_{T,L}(\omega, |\vec{q}|, T)$ are the transverse (T) and longitudinal (L) polarization functions of the photon in the isotropic primordial plasma. They depend on photon energy ω and momentum $|\vec{q}|$ and their temperature dependence is exposed by noting that

$\mathrm{Re}\,\Pi_{T,L} \propto \omega_{\rm p}^2$ where $\omega_{\rm p}$ is the plasma frequency; for the cases of interest $\mathrm{Im}\,\Pi_{T,L} \ll \mathrm{Re}\,\Pi_{T,L}$.

The consequences of these in-medium effects are two-fold. First, at high temperatures, they suppress the mixing angle since $\omega_{\rm p}^2 \sim \alpha T^2$ (in the relativistic limit), thereby diminishing contributions to thermal production for $T \gg m_V$. Second, the presence of the medium allows the production to proceed resonantly, whenever $\mathrm{Re}\,\Pi_{T,L}(T_r,\omega) = m_V^2$ [process (b) above]. Indeed, resonant conversion dominates the thermal dark photon abundance for $m_V < 2m_e$, but the constraints from direct detection experiments rule out the possibility of a thermal dark photon origin for 10 eV $\lesssim m_V <$ 100 keV altogether. The values of κ that are required for the correct thermal relic abundance, estimated in [3,28], are larger than the direct detection bounds discussed here by several orders of magnitude.

Dark photon dark matter remains a possibility when the relic density receives contributions from a vacuum condensate and/or from inflationary perturbations, process (c). The displacement of any bosonic field from the minimum of its potential can be taken as an initial condition, and during inflation any non-conformal scalar or vector field receives an initial contribution to such displacements scaling as $H_{\rm inf}/(2\pi)$, where $H_{\rm inf}$ is the Hubble scale during inflation. Even in absence of initial misalignment, the inflationary production of vector bosons can account for the observed dark matter density with a spectrum of density perturbations that is commensurate with those observed in the CMB [12]. While the production of transverse modes is suppressed, longitudinal modes can be produced in abundance [12],

$$\Omega_V \sim 0.3\sqrt{\frac{m_V}{1\ \mathrm{keV}}}\left(\frac{H_{\rm inf}}{10^{12}\ \mathrm{GeV}}\right). \tag{3}$$

For our mass range of interest the correct relic density would then be attained with $H_{\rm inf}$ in the 10^{12} GeV ballpark.

Undoubtedly, interactions between dark photons and the plasma are present, and the evolution of any macroscopic occupation number of vector particles is complicated by (resonant) dissipation processes [29]. For small enough couplings, these processes may be made inefficient, and most of the vector particles are preserved to form the present day DM. Equation (3) illustrates that—depending on the value $H_{\rm inf}$—a successful cosmological model amenable to direct detection phenomenology can always be found, and in the remainder of this work we assume that $\Omega_V h^2 = 0.12$, in accordance with the CMB-inferred cosmological cold dark matter density. Consequently, we also assume that the galactic dark matter is saturated by V-particles, and neglect any effects from substructure. The latter is a possibility when inflationary perturbations produce excess power on very small scales [12], and which will make the direct detection phenomenology ever more interesting. In this work, we restrain ourselves to the smooth dark matter density and hence to the time-independent part of the absorption signal.

2.2. Stellar dark photon constraints

In vacuum, this theory is exceedingly simple, as it corresponds to one new vector particle of mass m_V with a coupling $e\kappa$ to all charged particles. Some of this simplicity disappears once the matter effects for the SM photon become important, and the effective mixing angle becomes suppressed. The subtleties of these calculations, taking proper account of the role of the longitudinal modes of V, were fully accounted for only recently [30–33]. An understanding of these effects is important because they determine the exclusion limits set by the energy loss processes in the Sun, and other well-understood stars [34]. In the limit of small m_V (small compared to the typical plasma frequency in the central region of the Sun), the energy loss into vector particles scales as $\propto \kappa^2 m_V^2$, and is dominated by the production of longitudinal modes [30]. Although the resulting constraints from energy loss processes turn out to be quite strong in the $m_V \sim 100$ eV region, they weaken considerably for very small m_V, opening a vast parameter space for a variety of laboratory detection methods.

For $m_V > 10$ eV, dark matter experiments are sensitive enough to compete with stellar energy loss bounds if dark photons contribute to a significant fraction of the dark matter cosmological abundance. Here we review the most important aspects of stellar emission for the Stückelberg case, whereby we also update our previously derived constraint on horizontal branch (HB) stars.

Ordinary photons inside a star can be assumed to be in good local thermal equilibrium so that their distribution function is time independent, $\dot{f}_\gamma(\omega,T) = 0$. This allows one to relate photon production and absorption processes, $d\Gamma_\gamma^{\rm prod}/d\omega dV = \omega|\vec{q}|/(2\pi^2)e^{-\omega/T}\Gamma_\gamma^{\rm abs}$. In analogy, for the production rate of on-shell dark photons one has,

$$\frac{d\Gamma_{T,L}^{\rm prod}}{d\omega dV} = \kappa_{T,L}^2 \frac{\omega\sqrt{\omega^2 - m_V^2}}{2\pi^2} e^{-\omega/T}\Gamma_{\gamma,T,L}^{\rm abs}, \tag{4}$$

where $d\Gamma_{T,L}^{\rm prod}/d\omega dV$ is the rate of emission for a spin-1 vector particle with mass m_V and longitudinal (L) or transverse (T) polarization, while $\kappa_{T,L}^2$ is defined in (2). Inside active stars like our sun, the rate is dominated by bremsstrahlung processes; for explicit formulae see [30] and [32]. The expression (4) is useful since the optical theorem (at finite temperature) relates $\Gamma_{\gamma,T,L}^{\rm abs} = -\,\mathrm{Im}\,\Pi_{T,L}(\omega,\vec{q})/[\omega(1-e^{-\omega/T})]$.

Importantly, as alluded to above, emission can proceed resonantly when $m_V^2 = \mathrm{Re}\,\Pi_{T,L}$; see (2). In the emission of an on-shell dark photon, $\mathrm{Re}\,\Pi_L = \omega_P^2 m_V^2/\omega^2$ and $\mathrm{Re}\,\Pi_T = \omega_P^2$, up to corrections of $\mathcal{O}(T/m_e)$. A resonance inside a star occurs when either $\omega_P(r_{\rm res})^2 = \omega^2$ (longitudinal) or $\omega_P(r_{\rm res})^2 = m_V^2$ (transverse). The emission then proceeds from a spherical shell of radius $r_{\rm res}$ and the rates become independent of the details of the emission process. One may then integrate over the stellar profile by using the narrow width approximation [30,32],

$$\frac{d\Gamma^{\rm prod}}{d\omega} \simeq \left(\frac{2r^2}{e^{\omega/T(r)}-1}\frac{\sqrt{\omega^2-m_V^2}}{|\partial\omega_P^2(r)/\partial r|}\right)_{r=r_{\rm res}} \times \begin{cases} \kappa^2 m_V^2\omega^2 & \text{longitudinal,} \\ \kappa^2 m_V^4 & \text{transverse,} \end{cases} \tag{5}$$

for each polarization of transverse V-bosons. This form nicely exhibits the different decoupling behavior with respect to m_V. The bounds derived from stellar energy loss may qualitatively be understood on noting that the typical plasma frequency at the center of the star is given by,

$$\begin{aligned} \text{Sun:} &\quad \omega_P(r=0) \simeq 300\ \mathrm{eV}, \\ \text{Horizontal Branch:} &\quad \omega_P(r=0) \sim 2.6\ \mathrm{keV}, \\ \text{Red Giant:} &\quad \omega_P(r=0) \sim 200\ \mathrm{keV}, \end{aligned}$$

and both longitudinal and transverse resonant emission stops once $m_V > \omega_P(r=0)$. In our numerical analysis, we employ the full expressions for emission that also cover the case in which dark photons are emitted off-resonance.

The shaded regions in Fig. 1 are a summary of the astrophysical constraints on the mixing parameter κ that are independent of

the relic density of dark photon dark matter. The thin solid (dotted) gray lines show the constraints that are based solely on the emission of transverse (longitudinal) modes.

For the sun, the limit on the anomalous energy loss rate is identical to the one in previous work [30,32]. As a criterion we require that the luminosity in dark photons cannot exceed 10% of the solar luminosity, $L_\odot = 3.83 \times 10^{26}$ W. The limit is derived from observations of the ^{8}B neutrino flux; for details we refer the reader to the above references.

For Horizontal Branch (HB) stars, we update our own previously derived limit as follows (a similar limit has already been presented in [32]): as an HB representative, we consider a $0.8 M_\odot$ solar mass star with stellar profiles as shown in [34,35]. The energy loss is then limited to 10% of the HB's luminosity [34], for which we take $L_{\rm HB} = 60 L_\odot$ [35]. The transverse modes dominate the energy loss in HB stars. Since the corresponding resonant emission originates from one shell $r_{\rm res,\,T}$ for all energies, the derived constraint is sensitive to the stellar density profile in the resonance region $m_V < \omega_P(r=0) \simeq 2.6$ keV. For example, the kink visible in the thin gray line at $m_V \sim 150$ eV originates from entering the He-burning shell. Our result is in qualitative agreement with [32]; quantitative differences may be assigned to our use of full emission rate expressions [rather then (5)] that are integrated using Monte Carlo methods over the assumed stellar profile. In either case, such bounds are—by construction—only representative in nature and a detailed comparison of the derived limits will not yield much further insight.

Finally, the constraint that can be derived from Red Giant (RG) stars extends sensitivity to larger m_V. We require a dark photon luminosity that is less then 10 erg/g/s originating from the degenerate He core with $\rho \sim 10^6$ g/cm^3, $T \simeq 8.6$ keV [34]. Longitudinal emission dominates until transverse emission becomes resonant at $m_V = \omega_P({\rm core}) \sim 20$ keV. Here we note that there is room for improvement when deriving the limit from RG stars. For example, recent high-precision photometry for the Galactic globular cluster M5 has allowed the authors of [36] to derive constraints on axion-electric couplings and neutrino dipole moments that are based on the observed brightness of the tip of the RG branch. In conjunction with an actual stellar model, however, the better observations do not yield a drastic improvement of limits, as there appears to be a slight preference for extra cooling [36]. Albeit such hints to new physics are tantalizing, we in turn expect only mild changes to our representative RG constraint when a detailed stellar model is employed and/or better observational data is used; we leave such study for the future.

2.3. Constraints from $V \to 3\gamma$ decay

Next we consider constraints imposed by energy injection from γ-rays originating from $V \to 3\gamma$ decays below the e^+e^- threshold, for which the one-photon inclusive differential rate was computed in [3]. It reads,

$$\frac{d\Gamma}{dx} = \frac{\kappa^2\alpha^4}{2^7 3^7 5^3 \pi^3}\frac{m_V^9}{m_e^8}x^3\left[1715 - 3105x + \frac{2919}{2}x^2\right], \tag{6}$$

where $x = 2E_\gamma/m_V$ with $0 \le x \le 1$; the total decay width is obtained by integration, $\Gamma_{V\to 3\gamma} = \int_0^1 dx\, d\Gamma/dx$, and it sets the lifetime of dark photons for $m_V < 2m_e$.

A limit from observations of the diffuse γ-ray background was estimated in [28] by translating the results for monochromatic photon injection obtained in [37] and assuming a photon injection energy of $m_V/3$. Here we re-consider this limit and base it on the actual shape of the inclusive one-photon decay spectrum (6). Let dN/dE_γ denote the differential spectrum such that $\int dE_\gamma\, dN_\gamma/dE_\gamma = 3$. It follows that $E_\gamma(dN/dE_\gamma) = 3\Gamma^{-1}_{V\to 3\gamma} x(d\Gamma/dx)$.

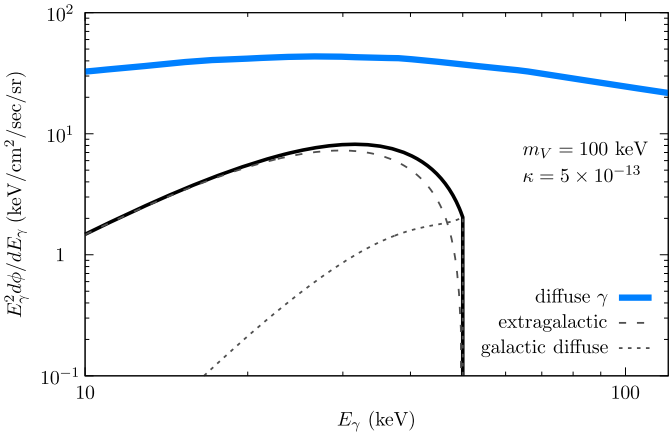

Fig. 2. Representative diffuse gamma ray bolometric flux (thick solid top line) together with computed extragalactic (galactic) photon fluxes depicted by the dashed (dotted) line from $V \to 3\gamma$ decay. We constrain the sum of these fluxes (solid line) to not exceed the observed one.

There are then two contributions to the diffuse photon background from $V \to 3\gamma$ decays. For the flux from the dark matter density at cosmological distances we find,

$$E_\gamma\frac{d\phi_{\rm eg}}{dE_\gamma} = \frac{\Omega_V \rho_c \Gamma_{V\to 3\gamma}}{4\pi m_V}\int_0^{z_f} dz\,\frac{E_\gamma}{H(z)}\frac{dN[(1+z)E_\gamma]}{dE_\gamma}, \tag{7}$$

where we have made the assumption that most of the dark matter has not yet decayed today, $\Gamma_V \ll H_0$, with H_0 being the present day Hubble rate. $H(z)$ is the Hubble rate at redshift z and we cut off the integral at the (blueshifted) kinematic boundary, $z_f = m_V/(2E_\gamma) - 1$, or, for $E_\gamma \to 0$, at some maximal redshift that is numerically inconsequential. In turn, the galactic diffuse flux is given by,

$$E_\gamma\frac{d\phi_{\rm gal}}{dE_\gamma} = \frac{\Gamma_{V\to 3\gamma}}{4\pi m_V}E_\gamma\frac{dN}{dE_\gamma}\rho_{\rm sol}R_{\rm sol}\mathcal{J}, \tag{8}$$

where $\mathcal{J}(\psi)$ is the $\rho_{\rm sol}R_{\rm sol}$-normalized line-of-sight integral at an angle ψ from the galactic center; $\rho_{\rm sol} \simeq 0.3$ GeV/cm^3 is the dark matter density at the sun's position, $R_{\rm sol} \simeq 8.3$ kpc away from the galactic center. For estimating the diffuse photon contribution, taking $\psi = \pi$ or $\pi/2$ yields $\mathcal{J} = 0.12$ or 0.2 for a NFW or an Einasto dark matter density profiles, and we take $\mathcal{J} = 0.15$ as fiducial value in (8).[1]

Fig. 2 depicts the representative diffuse gamma ray flux of photons (thick solid line) as taken from [37]. The extragalactic and diffuse galactic fluxes originating from dark photon decay with $m_V = 100$ keV and $\kappa = 5 \times 10^{-13}$ are respectively shown by the dashed and dotted lines. We constrain the flux contribution from dark photon decay by requiring that their sum (solid line) does not exceed 100% (10%) of the observed flux. The ensuing limits in the (m_V, κ) parameter space are shown in Fig. 1 and they constrain the region $m_V > 100$ keV. While the derived limit represents a conceptual improvement because use of the differential photon spectrum has been made, quantitatively, the strength of the limits is comparable to the previous estimate [28].

[1] In [37] $\mathcal{J}(\psi = \pi) = 1$ was taken. That choice would make the galactic diffuse flux dominate over the extragalactic one in Fig. 2, and strengthen the limit in Fig. 1.

The final constraint discussed in this section is due to precise measurements of the cosmic microwave background (CMB) radiation, and its sensitivity to DM decay. Specifically, $V \to 3\gamma$ decays at redshift $O(1000)$ alter the ionization history, raising TE and EE amplitudes on large scales, and damping TT temperature fluctuations on small scales. An energy density of

$$\frac{dE}{dV\,dt} = 3\zeta m_p \Gamma_{V\to 3\gamma} e^{-\Gamma_{V\to 3\gamma} t} \tag{9}$$

is injected into the plasma per unit time where $\zeta = (f/3)\Omega_V/\Omega_b$ is related to the injected energy per baryon, which is equal to $3\zeta m_p$; m_p is the mass of the proton and f denotes the overall efficiency with which the plasma is heated and ionized. In the case at hand $f = 1$. In [38] limits on the combination (ζ, Γ_V) were derived for decaying heavy dark photons with $m_V > 2m_e$, utilizing the Planck 2013 and WMAP polarization data. (For earlier analyses, see *e.g.* [39,40].) For lifetimes significantly longer than the cosmic time of recombination, the limit amounts to $\zeta\Gamma_V \lesssim 6\times 10^{-17}$ eV/s or $\tau_V \gtrsim 10^{26}$ s. We show this constraint in Fig. 1 and it is very comparable in sensitivity to the one derived from diffuse γ-ray lines.

3. DM absorption signals in direct detection experiments

3.1. Dark vector-induced ionization

If the energy of dark vectors is above the photoelectric threshold $E_V \geq E_{\rm th}$, atomic ionization becomes viable, for example in Xenon:

$$\text{Xe I} + V \to \text{Xe II} + e^-; \quad \text{Xe I} + V \to \text{Xe III} + 2e^-; \ldots \tag{10}$$

Here I's are used according to the usual atomic notation, and Xe I represents the neutral Xenon atom which is most relevant for our discussion. Most of the DM is cold and non-relativistic, so that $E_V = m_V$ with good accuracy. The astrophysics bounds, on the other hand, are often derived in the regime $E_V \gg m_V$. We will address the $E_V \simeq m_V$ case first, where the distinction between L and T modes all but disappears.

When $m_V \geq E_{\rm th} = 12.13$ eV, matter effects are not very important, and the problem reduces to the absorption of a massive nonrelativistic particle with $e\kappa$ coupling to electrons. The difference with the absorption of a photon with $\omega = m_V$ amounts to the following: the photon carries momentum $|\vec{q}| = \omega$, whereas the nonrelativistic dark vector carries a negligibly small momentum, $|\vec{q}| = m_V v_{\rm DM} \sim O(10^{-3})\omega$ where $v_{\rm DM}$ is the dark photon velocity. Fortunately, this difference has little effect on the absorption rate for the following reason. Both the photon wavelength and the DM Compton wavelength are much larger than the linear dimension of the atom, allowing for a multipole expansion in the interaction Hamiltonian, $(\vec{p}_e\vec{\epsilon})\exp(i\vec{q}\vec{r}_e) \simeq (\vec{p}_e\vec{\epsilon}) \times (1 + i\vec{q}\vec{r}_e + \ldots)$, where $\vec{\epsilon}$ is the (dark) photon polarization. The first term corresponds to the E1 transition that dominates over other multipole contributions, making the matrix elements for absorption of 'normal' and dark photons approximately equal. Accounting for the differences in flux, and averaging over polarization, gives the relation between the absorption cross sections [3]

$$\sigma_V(E_V = m_V) v_V \simeq \kappa^2 \sigma_\gamma(\omega = m_V) c, \tag{11}$$

where v_V is the velocity of the incoming DM particle. This relation is not exact and receives corrections of order $O(\omega^2 r_{\rm at}^2)$ where $r_{\rm at}$ is the size of corresponding electronic shell participating in the ionization process. Near ionization thresholds this factor varies from $\sim\alpha^2$ for outer shells to $\sim Z^2\alpha^2$ for inner shells. We deem this accuracy to be sufficient, and point out that further improvements can be achieved by directly calculating the absorption cross section for dark photons using the tools of atomic theory. (Analogous calculations have already been performed for the case of axion-like DM [41].)

Relation (11) is nearly independent of the DM velocity, and results in complete insensitivity of the DM absorption signal to the (possibly) intricate DM velocity distribution in the galactic halo; this is in stark contrast to the case of WIMP elastic scattering. The resulting absorption rate is given by

$$\text{Rate per atom} \simeq \frac{\rho_{\rm DM}}{m_V c^2} \times \kappa^2 \sigma_\gamma(\omega = m_V) c, \tag{12}$$

where $\rho_{\rm DM}$ is the local galactic DM energy density, and factors of c are restored for completeness.

The above formulae are sufficiently accurate provided all medium effects can be ignored. In general, however, the process of absorption of a dark photon must also account for the modification of $V-\gamma$ kinetic mixing due to in-medium dispersion effects. While the absorption of $m_V \gg E_{\rm th}$ particles cannot be affected significantly, close to the lowest threshold such effects can be important. To account for in-medium effects, we follow our original derivation in [31]. The matrix element for photon absorption $q + p_i \to p_f$ with photon four momentum $q = (\omega, \vec{q})$ and transverse (T) or longitudinal (L) polarization vectors $\epsilon_\mu^{T,L}$ is given by,

$$\mathcal{M}_{i\to f+V_{T,L}} = -\frac{e\kappa m_V^2}{m_V^2 - \Pi_{T,L}(q)} \langle p_f | J^\mu_{em}(0) | p_i\rangle \varepsilon^{T,L}_\mu(q). \tag{13}$$

Squaring the matrix element and summing over final states f, one obtains the absorption rate of L or T photons,

$$\begin{aligned}\Gamma_{T,L} &= \frac{1}{2\omega}(2\pi)^4\delta^{(4)}(q + p_i - p_f) e^2\kappa^2_{T,L}\varepsilon^*_\mu\varepsilon_\nu \\ &\quad\times \sum_f \langle p_i | J^\mu_{em}(0)|p_f\rangle\langle p_f|J^\nu_{em}(0)|p_i\rangle \qquad (14)\\ &= \frac{e^2}{2\omega}\int d^4x\, e^{iq\cdot x}\kappa^2_{T,L}\varepsilon^*_\mu\varepsilon_\nu \langle p_i|[J^\mu_{em}(x), J^\nu_{em}(0)]|p_i\rangle, \qquad (15)\end{aligned}$$

where the in-medium effective $V-\gamma$ mixing angle is given in (2). The polarization functions $\Pi_{T,L}$ are obtained from the in-medium polarization tensor $\Pi^{\mu\nu}$,

$$\begin{aligned}\Pi^{\mu\nu}(q) &= ie^2\int d^4x\, e^{iq\cdot x}\langle 0|T\, J^\mu_{em}(x) J^\nu_{em}(0)|0\rangle \\ &= -\Pi_T \sum_{i=1,2} \varepsilon_i^{T\mu}\varepsilon_i^{T\nu} - \Pi_L \varepsilon^{L\mu}\varepsilon^{L\nu}. \end{aligned}\tag{16}$$

Noting that

$$\begin{aligned}&\int d^4x\, e^{iq\cdot x}\langle 0|[J^\mu_{em}(x), J^\nu_{em}(0)]|0\rangle \\ &= 2\,\text{Im}\left[i\int d^4x\, e^{iq\cdot x}\langle 0|T\, J^\mu_{em}(x) J^\nu_{em}(0)|0\rangle\right],\end{aligned}\tag{17}$$

we can express the absorption rate in the lab-frame of the detector (14) as follows,

$$\Gamma_{T,L} = -\frac{\kappa^2_{T,L}\,\text{Im}\,\Pi_{T,L}}{\omega}. \tag{18}$$

This particular form is suitable for calculation, as we can relate $\Pi_{T,L}$ to tabulated optical properties of the material. For an isotropic and non-magnetic medium,

$$\Pi_L = (\omega^2 - \vec{q}^2)(1 - n^2_{\rm refr}), \quad \Pi_T = \omega^2(1 - n^2_{\rm refr}), \tag{19}$$

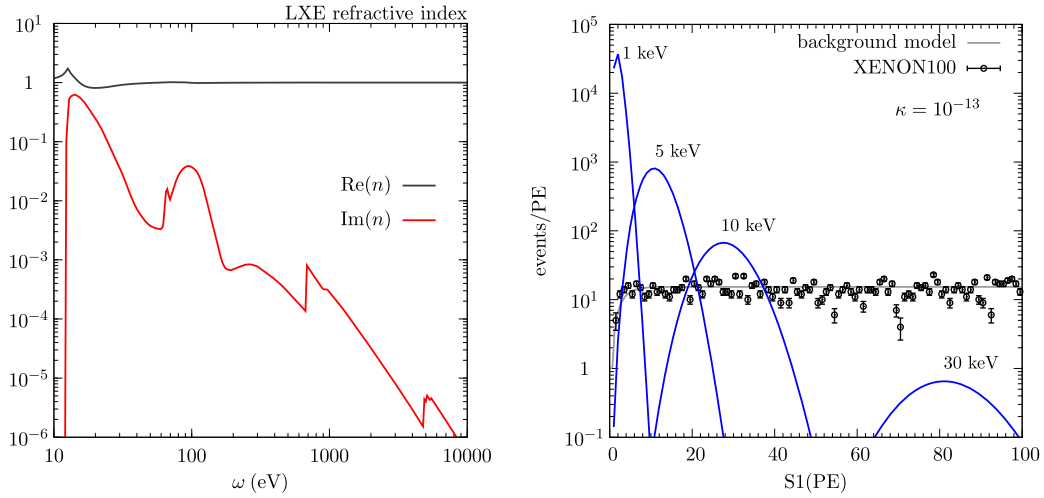

Fig. 3. *Left:* Real and imaginary parts of the liquid xenon refractive index computed from tabulated atomic scattering factors and using the Kronig–Kramers relation. Note that the maximum of the $\mathrm{Im}(n)$ function corresponds to the photoelectric cross section $\sigma_\gamma \sim 6 \times 10^{-17}$ cm^2. *Right:* Simulated events in 'xenon-units' of photo-electrons (PE) for various dark photon masses as labeled. Also shown are the reported event counts and the background model as taken from [24].

where n_{refr} is the (complex) index of refraction for electromagnetism. When $|\vec{q}| \ll \omega$, $\Pi_L = \Pi_T \simeq \Pi$, and all formulae for the absorption of L and T modes become idential, as expected.

As the final step, we obtain n_{refr} from its relation to the forward scattering amplitude $f(0) = f_1 + if_2$, where the atomic scattering factors $f_{1,2}$ are tabulated *e.g.* in [42]. Close to the ionization threshold we make use of the Kramers–Kronig dispersion relations to relate f_1 and f_2 in estimating n_{refr}. Alternatively, one may establish an integral equation relating the real and imaginary parts of ε; see [31].

When $m_V^2 \gg \Pi$, $\kappa_{L(T)} \simeq \kappa$, and the in-medium modification of absorption can be negelected. In that case the absorption rate per DM particle is

$$\Gamma \simeq \kappa^2 \omega \times \mathrm{Im}\, n_{\mathrm{refr}}^2 = \kappa^2 \sigma_\gamma \times \left(\frac{N_{\mathrm{at}}}{V}\right), \tag{20}$$

leading to the same formula for the absorption rate per atom as before, Eq. (12).

3.2. XENON10

The XENON10 data set from 2011 exemplifies the power of ionization-sensitive experiments when it comes to very low-energy absorption-type processes. With an ionization threshold of ~ 12 eV, the absorption of a 300 eV dark photon already yields about 25 electrons, and the relatively small exposure of 15 kg-days is still sufficient to provide the best limits on dark photons originating from the solar interior [31]. The same type of signature is used to provide important constraints on WIMP-electron scattering [43,44].

Despite significant uncertainties in electron yield, energy calibration, and few-electron backgrounds, we would like to emphasize the fact that *robust* and *conservative* limits can be derived which are independent of the above systematics. The procedure is straightforward, and follows the one already outlined in [31]. First, we count all ionization events (246) with up to 80 ionization electrons, or, equivalently, within 20 keV of equivalent nuclear recoil. If we do not attempt to subtract backgrounds (which is conservative), this implies a 90% C.L. upper limit of less than 19.3 dark photon absorptions per kg per day—irrespective of how many electrons are ultimately produced (as long as the number is less than 80). From that integral limit we derive the ensuing XENON10 dark photon dark matter constraint shown in Fig. 1. Remarkably, we observe that for 12 eV $\lesssim m_V \lesssim$ 200 eV the new limit is stronger than the previously derived solar energy loss constraint.

3.3. XENON100

The XENON100 collaboration has performed a low-threshold search using the scintillation signal S1 with an exposure of 224.6 live days and an active target mass of 34 kg liquid xenon [24]. A very low background rate of $\sim 5 \times 10^{-3}$/kg/day/keV has been achieved through a combination of xenon purification, usage of ultra-low radioactivity materials, and through self-shielding by volume fiducialization. In addition, with energy deposition in the keV range and above, the XENON100 experiment provides a sufficient energy resolution, allowing for mass reconstruction of a potential DM absorption signal.

We derive the signal in the XENON100 detector as follows. For the dark photon dark matter the kinetic energy is negligible with respect to its rest energy since $(v/c)^2 \sim 10^{-6}$. Therefore, a mono-energetic peak at the dark photon mass is expected in the spectrum. To derive the constraint, we first convert the absorbed energy m_V into the number of photo-electrons (PE) using Fig. 2 of Ref. [24]. This may result in a 10% uncertainty due to the corrections from binding energies of electrons at various energy levels as shown in Fig. 1 of Ref. [45]. We take into account the Poissonian nature of the process, and include the detector's acceptance as a function of S1, shown in Fig. 1 of Ref. [24]. The resulting S1 spectrum for various dark photon masses together with the reported data is shown in Fig. 3.

A likelihood analysis is used to constrain the kinetic mixing κ. The likelihood function is defined as

$$L(\kappa, m_V) = \prod_{i \geq 3} \mathrm{Poiss}(N^{(i)} | N_s^{(i)}(\kappa, m_V) + N_b^{(i)}) \,, \tag{21}$$

where i labels the bin number (which equals the number of S1 for each event) as shown in Fig. 6 of Ref. [24], $N_b^{(i)}$ and $N^{(i)}$ are the background and number of observed events as presented in Ref. [24]. Following the latter experimental work, we apply a cut S1 ≥ 3. Here we neglect the contribution from the uncertainty of n^{exp} to the likelihood function, since from Fig. 2 of Ref. [24] one can see that after we apply the S1 ≥ 3 cut, its influence on the limit of κ is less than 10%. A standard likelihood analysis then yields the resulting 2σ limit on κ as a function of m_V. It is shown

as the black dashed curve in Fig. 1. Again, we find the direct detection constraints to be very competitive with astrophysical bounds.

4. Discussion and conclusion

With an array of direct detection experiments now searching for signatures of elastic nuclear recoil of WIMPs on nuclei, and with sensitivity levels marching towards the neutrino background, it is important to keep in mind that other dark matter scenarios can also be sensitively probed with this technology. In particular, the exquisite sensitivity to ionization signatures at various experiments allows stringent constraints to be placed on generic models of super-weakly-interacting dark matter. In this paper, we have studied the sensitivity to the minimal model of dark photon dark matter, and obtained limits (summarized in Fig. 1) that exceed those from stellar physics over a significant mass range.

The sensitivity of current direct detection experiments already excludes dark photon dark matter with a thermally generated abundance. This is not a problem for the model, as the DM abundance may be determined by non-thermal mechanisms. For example, perturbations during inflation may create the required relic abundance [12], and further constraints on such models may be achieved if an upper bound on $H_{\rm inf}$ were to be established by experiments probing the CMB.

Dark photon dark matter has certain advantages over axion-like-particle dark matter with respect to direct detection. The absence of the dark photon decay to two photons removes the constraint from monochromatic X-ray lines. This latter signature usually provides a more stringent constraint on axion-like keV-scale DM than direct detection. Furthermore, the cross section for dark photons is significantly enhanced for small masses, relative to the cross section for absorption of axion-like particles.

The analysis presented in this paper addresses the model of a very light dark photon field, that is particularly simple and well-motivated. In addition, one could construct a whole family of 'simplified' models of very light dark matter, with observational consequences for direct detection [3]. The most relevant of these would involve couplings to electrons, and one could consider DM of different spin and parity:

$$\begin{aligned}&\text{(pseudo)scalar}\quad g_S S\bar{\psi}\psi,\quad g_P P\bar{\psi}\gamma_5\psi,\\ &\text{(pseudo)vector}\quad g_V V_\mu\bar{\psi}\gamma_\mu\psi,\quad g_A\mathcal{A}_\mu\bar{\psi}\gamma_\mu\gamma_5\psi,\\ &\text{tensor}\quad g_T T_{\mu\nu}\bar{\psi}\sigma_{\mu\nu}\psi,\ \cdots\end{aligned}\tag{22}$$

Here ψ stands for the electron field, g_i parametrizes the dimensionless couplings, and $V, \mathcal{A}, S, P, T\ldots$ are the fields of metastable but very long lived DM. The case considered in this paper corresponds to $g_V = e\kappa$, and the light mass m_V is protected by gauge invariance. However, even cases where the mass of DM is not protected by any symmetry are of interest, and can be considered within effective (or simplified) models. In this case, loop processes tend to induce a finite mass correction, which is at most $\Delta m_{\rm DMi} \sim g_i\Lambda_{\rm UV}$. With the cutoff $\Lambda_{\rm UV}$ at a TeV, it is natural to expect that, for a DM mass of $\sim$ 100 eV for example, one should have $g_i < 10^{-10}$. As demonstrated by the analysis in this paper, DM experiments can probe well into this naturalness-inspired regime, and set meaningful constraints on many variations of light DM models.

Finally, we would like to emphasize that further progress can be achieved through the analysis of 'ionization-only' signatures. For example, in noble gas- and liquid-based detectors one can improve the bounds for $E <$ keV by accounting for multiple ionization electrons (see Ref. [44]). The ionization of Xe atoms from the lowest electronic shells is likely accompanied by Auger processes, which generate further photo-electrons, and the corresponding bounds can be tightened. Analysis of these complicated processes may require additional input from atomic physics.

Acknowledgements

We would like to thank Fei Gao, Liang Dai, and Jeremy Mardon for helpful discussions. HA is supported by the Walter Burke Institute at Caltech and by DOE Grant DE-SC0011632. The work of MP and AR is supported in part by NSERC, Canada, and research at the Perimeter Institute is supported in part by the Government of Canada through NSERC and by the Province of Ontario through MEDT. JP is supported by the New Frontiers program of the Austrian Academy of Sciences.

References

[1] P. Cushman, C. Galbiati, D.N. McKinsey, H. Robertson, T.M.P. Tait, D. Bauer, A. Borgland, B. Cabrera, et al., arXiv:1310.8327 [hep-ex].
[2] K. Abazajian, S.M. Koushiappas, Phys. Rev. D 74 (2006) 023527, arXiv:astro-ph/0605271.
[3] M. Pospelov, A. Ritz, M.B. Voloshin, Phys. Rev. D 78 (2008) 115012, arXiv:0807.3279 [hep-ph].
[4] J. Preskill, M.B. Wise, F. Wilczek, Phys. Lett. B 120 (1983) 127.
[5] L.F. Abbott, P. Sikivie, Phys. Lett. B 120 (1983) 133.
[6] M. Dine, W. Fischler, Phys. Lett. B 120 (1983) 137.
[7] J. Jaeckel, A. Ringwald, Annu. Rev. Nucl. Part. Sci. 60 (2010) 405, arXiv:1002.0329 [hep-ph].
[8] T. Matos, A. Vazquez-Gonzalez, J. Magana, Mon. Not. R. Astron. Soc. 393 (2009) 1359, arXiv:0806.0683 [astro-ph].
[9] F. Piazza, M. Pospelov, Phys. Rev. D 82 (2010) 043533, arXiv:1003.2313 [hep-ph].
[10] A.E. Nelson, J. Scholtz, Phys. Rev. D 84 (2011) 103501, arXiv:1105.2812 [hep-ph].
[11] V.F. Mukhanov, H.A. Feldman, R.H. Brandenberger, Phys. Rep. 215 (1992) 203.
[12] P.W. Graham, J. Mardon, S. Rajendran, arXiv:1504.02102 [hep-ph].
[13] D. Horns, J. Jaeckel, A. Lindner, A. Lobanov, J. Redondo, A. Ringwald, J. Cosmol. Astropart. Phys. 1304 (2013) 016, arXiv:1212.2970.
[14] J. Jaeckel, J. Redondo, J. Cosmol. Astropart. Phys. 1311 (2013) 016, arXiv:1307.7181.
[15] P. Arias, A. Arza, B. Döbrich, J. Gamboa, F. Mendez, arXiv:1411.4986 [hep-ph].
[16] S. Chaudhuri, P.W. Graham, K. Irwin, J. Mardon, S. Rajendran, Y. Zhao, arXiv:1411.7382 [hep-ph].
[17] K. Arisaka, P. Beltrame, C. Ghag, J. Kaidi, K. Lung, A. Lyashenko, R.D. Peccei, P. Smith, et al., Astropart. Phys. 44 (2013) 59, arXiv:1209.3810 [astro-ph.CO].
[18] R. Bernabei, P. Belli, F. Montecchia, F. Nozzoli, F. Cappella, A. Incicchitti, D. Prosperi, R. Cerulli, et al., Int. J. Mod. Phys. A 21 (2006) 1445, arXiv:astro-ph/0511262.
[19] C.E. Aalseth, et al., CoGeNT Collaboration, Phys. Rev. Lett. 101 (2008) 251301; C.E. Aalseth, et al., CoGeNT Collaboration, Phys. Rev. Lett. 102 (2009) 109903 (Erratum), arXiv:0807.0879 [astro-ph].
[20] Z. Ahmed, et al., CDMS Collaboration, Phys. Rev. D 81 (2010) 042002, arXiv:0907.1438 [astro-ph.GA].
[21] R. Horvat, D. Kekez, M. Krcmar, Z. Krecak, A. Ljubicic, Phys. Lett. B 699 (2011) 21, arXiv:1101.5523 [hep-ex].
[22] E. Armengaud, Q. Arnaud, C. Augier, A. Benoit, A. Benoit, L. Bergé, T. Bergmann, J. Blümer, et al., J. Cosmol. Astropart. Phys. 1311 (2013) 067, arXiv:1307.1488 [astro-ph.CO].
[23] N. Abgrall, E. Aguayo, F.T. Avignone, A.S. Barabash, F.E. Bertrand, M. Boswell, V. Brudanin, M. Busch, et al., arXiv:1403.0475 [astro-ph.HE].
[24] E. Aprile, et al., XENON100 Collaboration, Phys. Rev. D 90 (2014) 062009, arXiv:1404.1455 [astro-ph.CO].
[25] K. Abe, et al., XMASS Collaboration, Phys. Rev. Lett. 113 (2014) 121301, arXiv:1406.0502 [astro-ph.CO].
[26] B. Holdom, Phys. Lett. B 166 (1986) 196; L.B. Okun, Sov. Phys. JETP 56 (1982) 502, Zh. Eksp. Teor. Fiz. 83 (1982) 892.
[27] R. Essig, J.A. Jaros, W. Wester, P.H. Adrian, S. Andreas, T. Averett, O. Baker, B. Batell, et al., arXiv:1311.0029 [hep-ph].
[28] J. Redondo, M. Postma, J. Cosmol. Astropart. Phys. 0902 (2009) 005, arXiv:0811.0326 [hep-ph].
[29] P. Arias, D. Cadamuro, M. Goodsell, J. Jaeckel, J. Redondo, A. Ringwald, J. Cosmol. Astropart. Phys. 1206 (2012) 013, arXiv:1201.5902 [hep-ph].
[30] H. An, M. Pospelov, J. Pradler, Phys. Lett. B 725 (2013) 190, arXiv:1302.3884 [hep-ph].
[31] H. An, M. Pospelov, J. Pradler, Phys. Rev. Lett. 111 (2013) 041302, arXiv:1304.3461 [hep-ph].
[32] J. Redondo, G. Raffelt, J. Cosmol. Astropart. Phys. 1308 (2013) 034, arXiv:1305.2920 [hep-ph].

[33] P.W. Graham, J. Mardon, S. Rajendran, Y. Zhao, Phys. Rev. D 90 (7) (2014) 075017, arXiv:1407.4806 [hep-ph].
[34] G.G. Raffelt, The Astrophysics of Neutrinos, Axions, and Other Weakly Interacting Particles, Univ. Pr., Chicago, USA, 1996, 664 p.
[35] D. Dearborn, G. Raffelt, P. Salati, J. Silk, A. Bouquet, Astrophys. J. 354 (1990) 568.
[36] N. Viaux, M. Catelan, P.B. Stetson, et al., Phys. Rev. Lett. 111 (2013) 231301.
[37] H. Yuksel, M.D. Kistler, Phys. Rev. D 78 (2008) 023502, arXiv:0711.2906 [astro-ph].
[38] A. Fradette, M. Pospelov, J. Pradler, A. Ritz, Phys. Rev. D 90 (2014) 035022, arXiv:1407.0993 [hep-ph].
[39] X.L. Chen, M. Kamionkowski, Phys. Rev. D 70 (2004) 043502, arXiv:astro-ph/0310473.
[40] J.M. Cline, P. Scott, J. Cosmol. Astropart. Phys. 1303 (2013) 044; J.M. Cline, P. Scott, J. Cosmol. Astropart. Phys. 1305 (E01) (2013) (Erratum), arXiv:1301.5908 [astro-ph.CO].
[41] V.A. Dzuba, V.V. Flambaum, M. Pospelov, Phys. Rev. D 81 (2010) 103520, arXiv:1002.2979 [hep-ph].
[42] B.L. Henke, E.M. Gullikson, J.C. Davis, At. Data Nucl. Data Tables 54 (2) (1993) 181.
[43] R. Essig, J. Mardon, T. Volansky, Phys. Rev. D 85 (2012) 076007, arXiv:1108.5383 [hep-ph].
[44] R. Essig, A. Manalaysay, J. Mardon, P. Sorensen, T. Volansky, Phys. Rev. Lett. 109 (2012) 021301, arXiv:1206.2644 [astro-ph.CO].
[45] M. Szydagis, A. Fyhrie, D. Thorngren, M. Tripathi, J. Instrum. 8 (2013) C10003, arXiv:1307.6601 [physics.ins-det].